Journal of Fluorescence
https://doi.org/10.1007/s10895-021-02842-w

ORIGINAL ARTICLE

Aesculetin Exhibits Strong Fluorescent Photoacid Character

Authors: Leah H. Knoor[1] · George R. Du Laney[1] · Isaac B. Jonker[1] · Liam P. Hoogewerf[1] · Yukun Tu[1] · Hunter T. Pham[1] · Joy Yoo[1] · Mark A. Muyskens[1]

Received: 30 August 2021 / Accepted: 18 October 2021

Abstract
Coumarins are bioactive molecules that often serve as defenses in plant and animal systems, and understanding their fundamental behavior is essential for understanding their bioactivity. Aesculetin (6,7-dihydroxycoumarin) has recently attracted attention due to its ability to act as an antioxidant, but little is known about its photophysical properties. The fluorescence lifetimes of its neutral and anion form in water are 19 ± 2 ps and 2.3 ± 0.1 ns, respectively. Assuming the short lifetime of the neutral is determined by ESPT, we estimate $k_{PT} \sim 5 \times 10^{10}$ s^{-1}. Using steady-state and time-resolved fluorescence spectroscopy, we determine its ground and excited-state pK_{a1} to be 7.3 and –1, respectively, making it one of the strongest photoacids of the natural coumarins. Aesculetin exhibits a strong pH dependence of the relative fluorescence quantum yield becoming much more fluorescent above pK_{a1}. The aesculetin anion has slightly photobasic character. We also report that aesculetin forms a fluorescent catechol-like complex with boric acid, and this complex has a pK_c of 5.6.

Keywords Photoacid · Fluorescence spectroscopy · Stokes shift · Quantum yield · Lifetime

Introduction

Aesculetin (6,7-dihydroxycoumarin, Scheme 1) is one of a host of bioactive compounds in the coumarin family. It is naturally produced in plants like the horse chestnut tree (*Aesculus hippocastanum*), and in addition to its recently characterized antioxidant activity [1], it has long been used in Chinese traditional medicine as an anti-inflammatory agent [2]. Coumarins in general serve a variety of functions in many organisms. In plants, they can be antifungal, antiviral, antioxidant, antibacterial, and more [3]. In humans and other animals, coumarins from dietary intake can have anticancer and anti-inflammatory effects [3]. Many coumarins are also fluorescent and can be used as biosensors [4, 5]. Chemically, coumarin derivatives can be substituted at any of 6 positions (Scheme 1a) on their bicyclic core structure, and the placement of substituents can have remarkable effects on fluorescence, acidity, and bioactivity [4, 6]. Aesculetin's two hydroxyl groups, adjacent on the benzene ring in a catechol-like functionality, involve intramolecular hydrogen bonding not found in other natural coumarins. Zhang and Wang emphasizes that the catechol moiety present in aesculetin has a notable effect on coumarin antioxidant behavior [4]. Furthermore, a study by Simkovitch and Huppert suggests that there may be a direct relationship between a coumarin derivative's photoacidity and its physiological roles [7].

Many natural coumarins become much stronger acids after absorbing light and are thus classified as photoacids; umbelliferone (7-hydroxycoumarin) and scopoletin (6-methoxy-7-hydroxycoumarin) are prominent examples [7, 8]. In the case of a fluorescent photoacid, this increase in acidity may be observed directly from steady-state fluorescence spectroscopy. Here we use pK_a to characterize a compound's acidity: pK_a is the negative decimal logarithm of the aqueous acid ionization equilibrium constant, K_a, and is also the pH at which half of the molecules in solution will be the neutral species while the other half will be ionized. Figure 1 shows the fluorescence excitation and emission spectra of aesculetin at a pH below and above the pK_a. While the excitation spectrum reveals a large shift in absorbance with pH, the peak wavelength of the fluorescent emission remains nearly unchanged. We can observe neutral aesculetin fluorescence by placing it in a solvent that is expected to have a much slower proton transfer, such as methanol, represented by the green trace in Fig. 1, and we observe anion emission at high pH. Excitation of the neutral form in water,

✉ Mark A. Muyskens
mark.muyskens@calvin.edu

[1] Calvin University, 3201 Burton St SE, Grand Rapids, MI 49546, USA

Published online: 17 November 2021

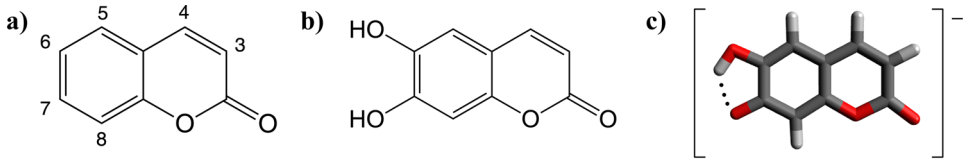

Scheme 1 **a**) Coumarin core structure with numbering scheme, **b**) aesculetin (6,7-dihydroxycoumarin), neutral form **c**) aesculetin-anionic conformer indicating a hydrogen bond (dotted line) formed by the donor OH in position 6

which is present below the pK_a, produces emission that bears a strong resemblance to anion emission. This is consistent with photoacid behavior, where, after absorbing light, most of the excited-state neutral molecules become excited anions by transferring a proton to the solvent before fluorescence occurs.

A compound's photoacid behavior can be described by its ground-state pK_a and excited-state pK_a^*. Steady-state absorbance spectroscopy is one of many methods used to determine both pK_a [9] and pK_a^*, provided the substance remains fluorescent in the region of the pK_a^* as demonstrated with scopoletin [8]. The emission spectra of scopoletin reflect a straightforward acid–base equilibrium in the excited state as well. Aesculetin's fluorescent emission below its pK_a becomes very weak, complicating the steady-state approach to pK_a^*. Instead, we use time-resolved fluorescence spectroscopy (TRF) to provide direct observation of excited-state proton transfer (ESPT), yielding a rate constant for the process. Furthermore, the kinetic isotope effect can be observed by replacing water with D_2O, which deuterates the acidic proton, slowing proton transfer and supporting the idea that ESPT plays a role in the excited state dynamics. If proton loss results in or is coordinated with proton gain at the carbonyl group, the aesculetin tautomer is formed in a process often called excited-state intramolecular proton transfer (ESIPT). The excited-state tautomer is expected to be observed as emission at longer wavelengths than the anion, as shown in umbelliferone and 4-methylumbelliferone fluorescence [10, 11] and our computational modeling discussed below. The pH 4 aesculetin emission in Fig. 1 (solid red trace) shows that the excited-state neutral, anion and tautomer all play a role.

Recently, two coumarins that are di-oxygenated on the benzene ring at positions 6 and 7 have been characterized: scopoletin [8, 12] and 4-methylaesculetin [12] where the latter

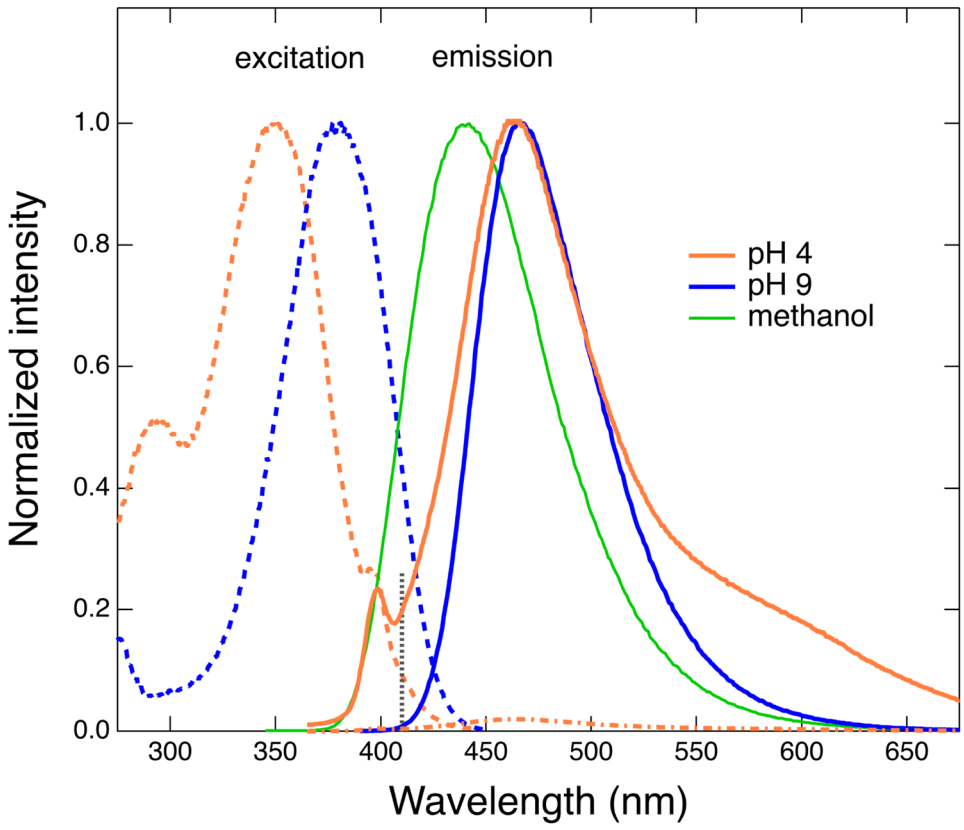

Fig. 1 Fluorescence excitation (dashed) and emission (solid) spectra of aesculetin in methanol (green trace), pH 4 buffer (red traces) and pH 9 buffer (blue traces), illustrating fluorescent photoacid behavior; the dot-dash trace is the pH 4 emission without normalization and scaled relative to the pH 9 trace; the water Raman peak is visible near 400 nm in the low pH spectra; the vertical dotted line at 410 nm highlights a wavelength in a region where we predict neutral aesculetin emission to occur with minimal anion emission in aqueous solution

is expected to have many similar characteristics to aesculetin. Little has been reported about the photophysical properties of aesculetin. The only prior pK_a value reported for aesculetin [13] is complicated by the presence of borate ion. Our study describes aesculetin's properties of pK_a, pK_a^*, fluorescence lifetime, quantum yield, and ESPT rate constant using steady-state and time-resolved fluorescence spectroscopy.

Materials and Methods

Aesculetin (Indofine Chemical Company, Inc., 99 + %) purity was verified by nuclear magnetic resonance spectroscopy, HPLC and LC–MS analysis and used without further purification. Solutions with concentrations of 20 µM were prepared using appropriate non-fluorescing and non-quenching buffers (0.1 M sodium citrate, potassium dihydrogen phosphate, glycine, and sodium bicarbonate), with pH ranging from 1 to 12. The influence of borate in solution was observed using 0.1 M borate buffer and the Britton-Robinson buffer system (~0.04 M borate ion and constant 0.1 M ionic strength [14]. The pH meter (Accumet AR15) was standardized to reference solutions at pH 1.67, 4.00, 7.00, 10.00 and 13.0 where appropriate. Steady-state absorption and emission spectra were collected on a UV–Vis spectrophotometer (Varian Cary 50, Cary 100 Bio, and Hitachi U3900H) and spectrofluorometer (Horiba FluoroMax-4). Emission spectra were obtained with an excitation wavelength near the 354-nm isosbestic point. Samples were not purged of dissolved oxygen because the presence of oxygen was observed not to influence the fluorescent emission properties of aesculetin. This system is modeled as having two absorbing species, neutral N and anion A, absorbing at two distinct maximum wavelengths, λ_N and λ_A, respectively. The anion-dianion equilibrium occurs in a pH region sufficiently different from the neutral-anion equilibrium region to allow analogous analysis. The pK_a is determined by fitting a sigmoid function to the maximum absorbance wavelength, λ´, versus pH, where λ´ represents the absorbance maximum wavelength in the spectrum. The sigmoid relationship:

$$\lambda' = \lambda_N + (\lambda_A - \lambda_N)/(1 + 10^{(pK_a - pH)})$$

is derived from the Henderson-Hasselbalch equation, and the pH at the midpoint of the sigmoid curve is the pK_a. Measurements at pH above 11 were taken immediately after mixing to minimize effects of ring opening [13].

Quantum Yield Determination

A quantitative determination of the quantum yield was carried out relative to the standard quinine sulfate (QS, 0.1 N H_2SO_4, 22 °C) [15] using 350-nm excitation for all solutions. The absolute fluorescence quantum yield of aesculetin is $\Phi_A = \Phi_Q(I_A/I_Q)(A_Q/A_A)(n_S/n_W)^2$, where Φ_Q is 0.577 for QS, I_A/I_Q is the ratio of the wavelength-integrated fluorescence intensity of aesculetin to quinine sulfate, A_Q/A_A is the ratio of the absorbance of QS to aesculetin at 350 nm, and n_S/n_W is the ratio of refractive indices of the aesculetin solution solvent and water. This analysis is performed with 4–5 absorbances over a range from 0.01 to 0.11 and yields the expected linear increase in the integrated intensity with increasing absorbance. In addition, the relative quantum yield across a pH range is determined by the integrated emission intensity normalized by absorbance at the excitation wavelength, assuming that the emission spectra are taken at the same solution concentration, excitation wavelength, excitation intensity and emission sensitivity.

Time-Resolved Fluorescence

The equipment used for time-resolved fluorescence data collection is described in detail in a recent paper from our lab [8]. The system uses a picosecond laser light source producing 5-ps pulses of 350-nm light and time-correlated single photon counting (TSCPC) detection. Average laser power at the sample is 1 mW or less, and the instrument response function for this system is ~ 40 ps. The time-resolved fluorescence decays in D_2O use a 0.1 M citrate buffer around pH of 4.8 (4.3 in H_2O) for both aesculetin and umbelliferone at 10 µM.

Computational Methods

All quantum chemistry modeling using density functional theory (DFT) were performed with the Gaussian 16 program package [16] and the WebMO Pro interface [17]. Full geometry optimizations of aesculetin (neutral and anion) in water were performed for the ground state using the functional B3LYP, the 6-31G(d) basis set and the SMD-UAKS solvation model as implemented in Gaussian 16 to represent a diffuse dielectric medium of the solvent. Care was taken to ensure each ground state structure was at a global minimum energy, which for the neutral structure involves an intramolecular hydrogen bond of the acidic proton to the oxygen at position 6. Comparison calculations using CAM-B3LYP functional and 6–311 + + G(2d,p) basis set were done to check consistency of results. To model the excited state, the time-dependent DFT/B3LYP/6-31G(d)/SMD-UAKS method was used; the predicted absorbance wavelength comes from the un-optimized and optimized excited state TD-DFT computation to model the vertical excitation and the fluorescent emission, respectively.

Results and Discussion

Absorbance and Ground State pK_a

Aesculetin has a large, 40-nm red-shift in its absorbance maximum wavelength as pH is increased from 3 to 9. This is consistent with an acid–base equilibrium between neutral aesculetin and its anion. Fig. S1 shows the pH-dependent absorbance spectra with isosbestic points at 278 and 354 nm. Figure 2 shows the dependence of the absorbance maximum wavelength on pH without borate ion present (trace a) and in the presence of borate ion (trace b). The midpoint of the sigmoid curve fitted to trace-a indicates a pK_{a1} of 7.3 ± 0.1. Figure 2 trace b shows a pK_c of 5.6 ± 0.1 in the presence of 0.04 M boric acid using the Britton-Robinson buffer (containing borate, citrate, and phosphate buffer systems); K_c being the formation equilibrium constant for the aesculetin boric acid complex, ABC. The Fig. 2 inset shows the pH 8 aesculetin absorbance spectra with and without the presence of boric acid (pK_a 9.14 at 25 °C) compared to a low pH absorbance spectrum. This difference between pK_{a1} and pK_c due to the presence of boric acid is likely the result of a complex formed by boric acid interaction with the catechol-like functionality of aesculetin, creating a compound that is also fluorescent (Scheme 2). The pK_c of ABC is in good agreement with the previously reported pK_{a1} for aesculetin (5.4), which was determined using the Britton-Robinson buffer system [13]. The ABC pK_c is also in good agreement with the pK_c of 5.0 characterizing the complexation of boric acid with catechol [18]. This complexation interaction raises the question of whether a similar interaction will form between boric acid and other vicinal dihydroxycoumarins, namely daphnetin (7,8-dihydroxycoumarin) and 5,6-dihydroxycoumarin, which is the focus of an ongoing study. A preliminary estimate of the fluorescence quantum yield for daphnetin is that it is more than a hundred times less efficient than quinine sulfate, making the experimental study more challenging.

An aesculetin ground-state pK_a of 7.3 agrees well with the reported pK_a of 7.1 for 4-methylaesculetin, a compound like aesculetin with the addition of a methyl group in position 4 [12]. It has been shown that the

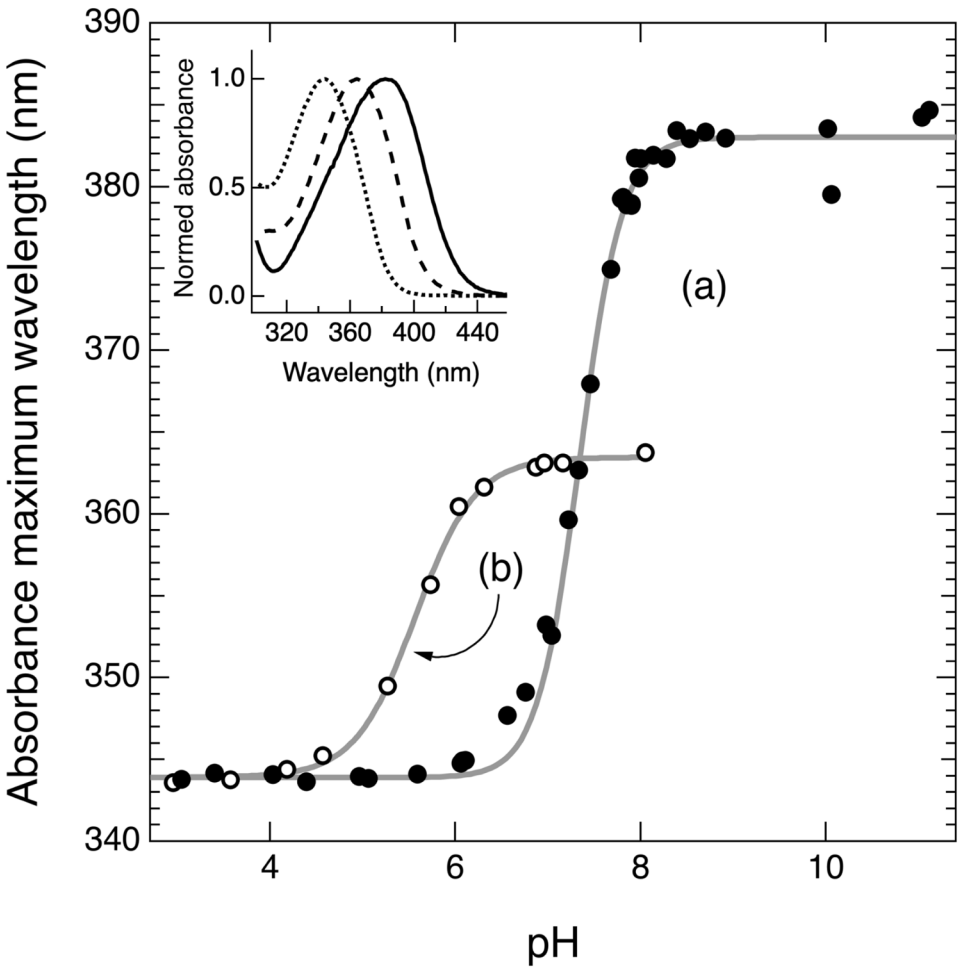

Fig. 2 pH dependence of the absorbance maximum wavelength for aesculetin in (**a**), solid symbols, 0.1 M non-borate buffers and (**b**), open symbols, 0.1 M buffer with borate present; solid lines are sigmoid fits to the data with pH midpoints of 7.3 and 5.6 for curve a and b, respectively; the inset shows normalized absorbance spectra where the dotted trace is pH 3.0, the dashed trace is pH 8.0 borate buffer, and solid trace is pH 8.0 non-borate buffer

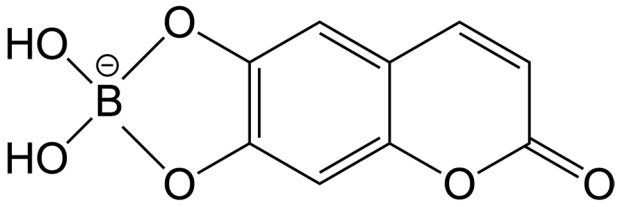

Scheme 2 Borate complex with aesculetin

presence of a 4-methyl group has little influence on pK_a in the case of umbelliferone and 4-methylumbelliferone [19, 20], and recent data from our lab on grevillone (6-hydroxycoumarin) and 4-methylgrevillone (4-methyl-6-hydroxycoumarin) indicate that the methyl group does not have a significant effect on the pK_a of grevillone. A pK_a of ~ 7 compares well to scopoletin with pK_a 7.4 [8, 12]. It appears that the oxygen in position 6 common to aesculetin and scopoletin slightly lowers the pK_a compared to umbelliferone, mono-oxygenated in position 7, having a pK_a ~7.8 [19]. The only calculated pK_a for aesculetin, using a linear correlation with semi-empirical thermodynamic quantities, is 6.9, [21] which is reasonably close to our experimental value and predicts that ionization occurs at position 7.

Figure 3 shows the pH influence on the absorbance maximum wavelength over a wider span of pH revealing the second ionization pK_{a2} above pH 12. Fig. S1c shows the pH-dependent absorbance spectra of the anion and dianion with isosbestic points at 324 and 404 nm, characteristic of an acid–base equilibrium. The sigmoid fit in Fig. 3 gives a pK_{a2} for aesculetin of 12.45 ± 0.15. To ensure that the spectra are not skewed by lactone ring opening at high pH, we minimized the time between adding stock solution aliquots to buffers and recording spectra. Our experimental pK_{a2} value is in good agreement with the 4-methylaesculetin pK_{a2} value of 12.2 reported by Pina et al. [12].

Fluorescence and pK_a^*

Figure 3 also shows the pH influence on the fluorescence maximum wavelength over a wide pH range, revealing regions where anion and dianion dominate the emission,

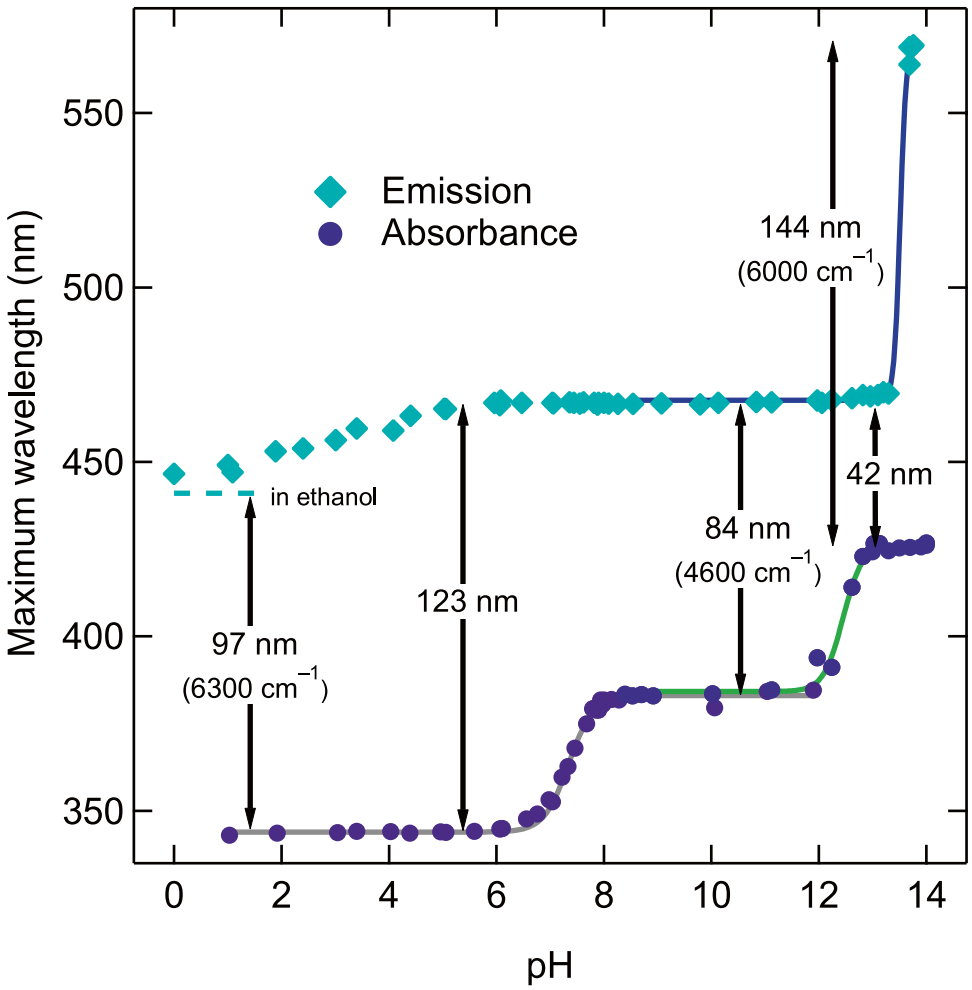

Fig. 3 Absorbance (circle markers) and emission (diamond markers) maximum wavelength dependence on pH. Smooth curves are sigmoid fits to the data in the vicinity of the corresponding pK$_a$; vertical arrows indicate the Stokes shift at corresponding pH; the Stokes shift at ~5.5 is expanded due to photoacid behavior, namely absorbance by the neutral and emission by the anion due to excited state proton transfer; at pH 13, the Stokes shift is decreased to 42 nm due, in this case, to photobase behavior

namely pH regions 6–13 and near 14, respectively. The dianion emission is considerably red shifted with a maximum wavelength of 569 nm. Figure 3 shows that the transition from anion to dianion emission occurs at pH 13.5 ± 0.2, which is pK^*_{a2} (the pK^*_a of the anion). Since this value is slightly larger than pK_{a2}, we can describe the anion as being weakly photobasic, most notable at around pH 13, where the dianion is the absorbing species acquiring a proton from the solvent and emission is from the anion. In terms of pH accuracy above pH 13, we note that the ionic strength in this region is necessarily increasing above 0.1 M and the pH reading is being made outside our pH probe calibration range. The emission intensity at pH 13.7 is primarily dianion and is seven times less than the anion emission intensity at pH 13.0 when normalized for absorbance at the excitation wavelength of 406 nm. One consequence of this disproportion in emission intensity is that the sigmoid-fitting approach based on the maximum emission wavelength is biased towards the weaker emitter, in this case making pK^*_{a2} too large by about ~0.1. Our estimated uncertainty in pK^*_{a2} of ± 0.2 takes both this bias and pH accuracy into account. The ring-opening kinetics can be observed at pH 14, illustrated by the absorbance peak diminishing by ~33% over 10 min at room temperature (22 °C); thus, spectra taken within the first several minutes of making the solution should not be compromised by the decomposition. Figure 3 also shows a more gradual transition in emission maximum wavelength from anion to neutral. This region has a greatly diminished quantum yield, as discussed below, and a varying contribution by the phototautomer, making this transition less distinct and unable to clearly show pK^*_{a1}.

Figure 3 shows the Stokes shifts of the neutral, anion and dianion. In the pH region just below pK_{a1}, aesculetin has a larger-than-expected Stokes shift due to its photoacid behavior. Near pH 13 the anion has a dramatically smaller Stokes shift, in this case, due to photobase behavior.

Although the absorbance spectra of aesculetin-borate complex anion (ABC) and the aesculetin anion are different (Fig. 2 inset), the emission maximum wavelengths are very close, 466 and 467 nm, respectively. Table 1 summarizes the spectral comparison of these two species. While the full-width-half-maximum (FWHM) of the absorbance bands are quite similar, the FWHM of the ABC emission band is 30% wider than aesculetin anion emission. This means the most sensitive fluorescent spectral indication of the ABC is necessarily based on emission band width. The ABC exhibits a much larger Stokes shift than aesculetin anion. We comment on the relative quantum yield and lifetime of the aesculetin borate complex anion in the respective sections below.

Table 2 Quantum yield of aesculetin in water and alcohols

Species	Solvent index of refraction at 350 nm	Relative quantum yield [a]	Quantum yield
Aesculetin (pH 9.3)	1.3490	0.40 ± 0.02	0.23
Aesculetin in methanol	1.3437	0.3 ± 0.05	0.18
Aesculetin in ethanol	1.3802	0.58 ± 0.02	0.32

[a]relative to quinine sulfate quantum yield of 0.577 in 0.1 N H_2SO_4 at 22 °C, [15]

Quantum Yield

Many natural coumarins are more fluorescent in their anionic (high pH) form [22]. Scopoletin and umbelliferone, for example, have quantum yields of 0.63 at pH 9 [8] and 0.91 at pH 9.5 [23], respectively. Table 2 provides the quantum yield determination of aesculetin in water, methanol, and ethanol relative to the standard quinine sulfate. These data are the result of five determinations establishing a relative uncertainty of less than 10% (see Fig. S2). While aesculetin is not as efficient as umbelliferone and scopoletin, it yields a bright fluorescence at high pH.

Figure 4 shows the quantum yield across a wide pH range found by determining the relative quantum yield from integrating the emission spectra (see Fig. S3a), normalized by the measured absorbance at the excitation wavelength and then scaled to the absolute quantum yield in Table 2. The quantum yield at pH 4 is ~ 80 times lower than at pH 9.3 (see Fig. 1 unnormalized pH 4 trace). We note the strong resemblance of Fig. 4 to the pK_a curve in Fig. 2, which makes aesculetin remarkably different in comparison to scopoletin and umbelliferone. In the latter cases, the

Table 1 Comparison of aesculetin anion and ABC spectral characteristics

	Absorbance			Emission			
Species	Maximum wavelength (nm)	Band FWHM (nm)	Band FWHM (cm^{-1})	Maximum wavelength (nm)	Band FWHM (nm)	Band FWHM (cm^{-1})	Stokes shift (cm^{-1})
Aesculetin anion (pH 9)	384	60	4200	467	67	3000	4600
Aesculetin-boric acid complex	362	58	4500	466	88	3900	6100

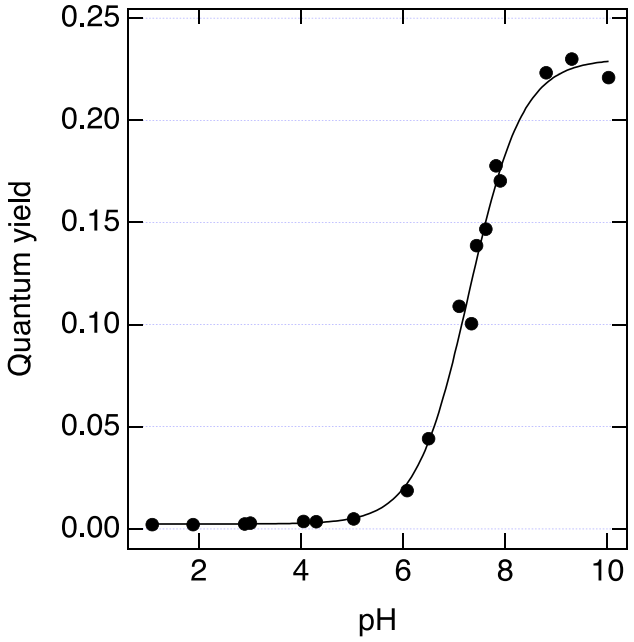

Fig. 4 pH dependence of the quantum yield of aesculetin (in borate-free, 0.1 M aqueous buffers); the midpoint of the sigmoid fit is 7.30; the maximum point in the series is normalized to the aesculetin quantum yield given in Table 2

relative quantum yield changes only modestly across the pK_a region. Scopoletin's quantum yield decreases by only about 15% below its pK_a (7.4) [8]; and the report by Zhang et al. [23] and unpublished data from our lab indicates the relative quantum yield of umbelliferone changes by less than 15% over the range 4 to 11, well above and below its pK_a. Above the pK_{a1}, quantum yield of aesculetin appears to have a maximum around pH 9 and drops off above 11. Opening of the α-pyrone ring becomes a consideration above pH 12.

A reduced quantum yield may be related to an increased role of nonradiative channels due to several considerations, triplet states, quenching and structural flexibility of aesculetin. The process of intersystem crossing to a nearby triplet state may account for a significant nonradiative decay channel. TD-DFT calculations of aesculetin neutral at the B3LYP/aug-cc-pVTZ/SMD(H_2O) level of theory to compare the energy of the optimized triplet excited state, T_2, to the optimized singlet state, S_1, suggest there is a large enough energy gap (~ 70 kJ/mol) that ISC may not play a significant role in draining population from the S_1 state. A significant quenching channel by the geminate proton is used in modeling the excited state dynamics of 1-naphthol [24], which is a well-studied photoacid having a comparable pK_a^* to aesculetin. However, the reduction in quantum yield of the naphtholate anion that can be attributed to this quenching effect is at most ~ 35%, whereas we observe what appears to be more than a 90% reduction in the quantum yield of aesculetin.

The shift in quantum yield coincides with the transition from the neutral form with two vicinal hydroxyl groups to the anion with only one hydroxyl group due to deprotonation. Non-rigid groups on a fluorophore can contribute to a significant nonradiative decay path, for example, increased amino group motion in amino coumarins is tied to lowered fluorescence efficiency [25]. Large substituent rotational flexibility on a rigid fluorophore contributes to a relatively large nonradiative decay rate, reducing the fluorescence quantum yield [15]. At the same time, hydrogen bonding involving the hydroxyl groups in aesculetin may play a role in stabilizing both the neutral and anion conformers. In the anion, ionization is expected in position 7 and the OH in position 6 then is a H-bond donor held in the plane of the coumarin to some extent by the H-bond. In the neutral form, a hydrogen bond can involve either OH in the role of donor, and the question centers on what barriers exist to rotation of the vicinal OH groups on the benzene ring. In the neutral form it is possible to have less a restricted, 'free' hydroxyl group motion, whilst the other OH is held in the coumarin plane by a H-bond; on the other hand, even monohydroxy-coumarins have some OH rotation restriction mentioned in the next section. Furthermore, isomerization may occur where both hydroxyl groups interchange dihedral angles and swap hydrogen bonding roles. The question of whether one or the other planar, hydrogen-bonded conformer of aesculetin neutral is preferred, is answered by modeling at several DFT levels of theory that predicts the two conformers are nearly equal in energy (< 1 kJ/mol). More OH flexibility in the neutral form compared to the anion may account in part for why the quantum yield would decrease below the pK_a.

To support the idea that OH flexibility may be tied to the relative quantum yield dependence on pH, we used DFT modeling to predict barriers to hydroxyl group rotation for the neutral and the anion. Figure 5 shows the energy dependence on OH dihedral angle in two cases, for aesculetin neutral and anion. These are cross sections to a three-dimensional potential energy surface (PES) described in more detail in the SI. To model the aqueous phase, we use the SMD formalism specifying a diffuse dielectric medium consistent with water surrounding the dipolar molecular structure, which lacks any accounting for explicit hydrogen-bonding interactions of aesculetin with surrounding water molecules. As such, these model results are a partial representation of the energetic dependence on OH rotation. Our modeling as presented in Fig. 5 predicts OH rotation in the anion is restricted by a larger barrier than the neutral, which is qualitatively consistent with the experimental relative quantum yield. Modeling at several DFT levels of theory give the same relative result. The σ_1 curve in Fig. 5 begins with a hydrogen bonded conformer at 180°, places the two OH groups closest to each other at the mid-point, and has an unexpected local minimum near the midpoint. The barrier

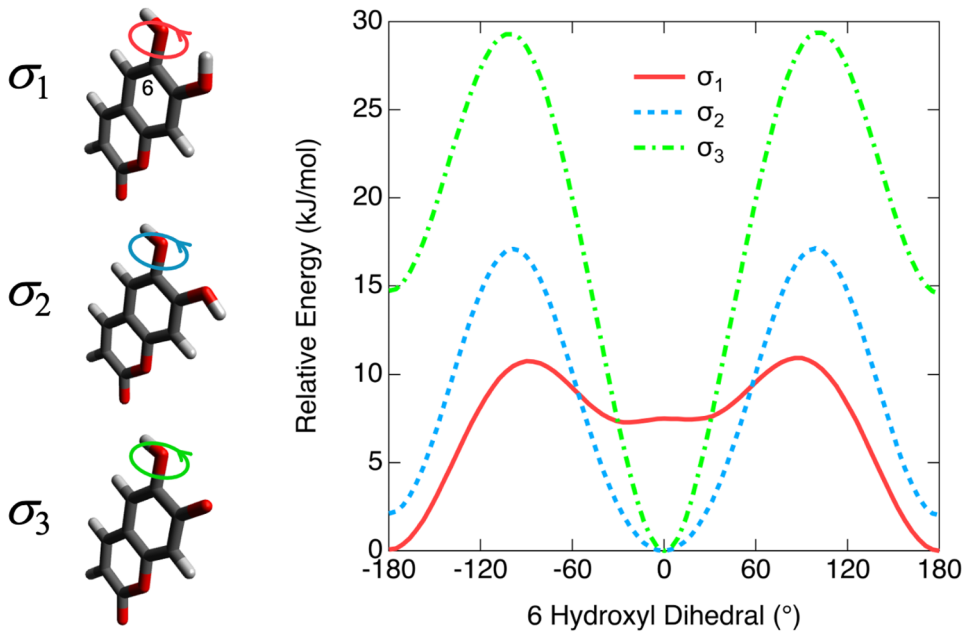

Fig. 5 Barriers to OH rotation for aqueous aesculetin neutral and anion showing relative energy with respect to the dihedral angle of O6H (OH in the 6-position of the coumarin structure), (σ_1) solid, red trace, O6H dihedral rotation holding O7H dihedral constant (the starting conformation for this trace is O7H as the H-bond donor as shown in left panel, O6H dihedral is –180°); (σ_2) dashed, blue trace, O6H dihedral rotation holding O7H dihedral constant (in this trace, O6H is the H-bond donor at the mid-point of the blue trace where the O6H dihedral is 0°); and (σ_3) dot-dash, green trace, dihedral rotation with position-7 O deprotonated (O6H is the H-bond donor at the mid-point of the green trace where O6H dihedral is 0°); modeling is at the B3LYP/6-31G(d)/SCRF(SMD, Solvent = Water, Radii = UAKS) level of theory, coordinate-scans optimizing structure at specified dihedral angles

in this potential energy curve at 90° may reveal the effect of compromising the overlap of the oxygen atomic orbitals with the key delocalized molecular orbitals, the HOMO and LUMO, due to rotation of the oxygen atom orbitals out of the coumarin plane. To be sure, comparing OH dihedral angle coordinate scan for 7-hydroxycoumarin (umbelliferone), 6-hydroxycoumarin (grevillone), and cyclohexanol reveals a much higher barrier for the coumarin hydroxyl rotation than the rotation about a C(sp3)–O(sp3) bond as represented by cyclohexanol (see Fig. S6). A further consideration is the hydroxyl flexibility in the electronic excited state, a next step in modeling that is beyond the scope of the current study. As a side note, an interesting observation in the gas-phase PES of aesculetin neutral is a concerted motion channel where OHs move in opposite dihedral directions to isomerize between the H-bonded conformers. While this concerted channel, present also in the PES calculated for the non-polar solvent cyclohexane, is the lowest barrier to OH rotation in the gas phase, the lowest energy channel in the aqueous phase is represented by σ_1 in Fig. 5. In all models, the barriers to OH rotation are lower for the neutral than the anion.

At low pH, the drop in aesculetin fluorescence quantum yield combined with emission from multiple excited-states makes the direct steady-state fluorometric observation of the pK_a^* complicated. Fig. S3a shows emission spectra over the pH range 0–6 (below pK_{a1}) further illustrating the steep decline in emission intensity and the normalized spectra reveal that both neutral (N*) and phototautomer (T*) contribute to the emission spectrum at low pH. Time-resolved emission of the aesculetin neutral discussed in the next section to provides another approach to determining the pK_{a1}^*. 4-methylaesculetin exhibits a similar dramatic change in fluorescence intensity [12] in the region of pK_{a1}, which is interpreted as indicating a pK_a^* close to its pK_a, however given the similarities of methylaesculetin and aesculetin fluorescence, the observed emission intensity decrease is likely due to a change in relative quantum yield like aesculetin. The role of the phototautomer in aesculetin excited state dynamics in water is apparently a minor one. Fig. S3b shows that in the pH range below the pK_a, the phototautomer has a maximum emission relative to the anion peak of about 30% at ~ pH 1 diminishing in relative intensity as pH increases up to the pK_a. The role of the phototautomer also decreases as pH drops from 1 to 0, the latter pH being close to the pK_{a1}^* estimated from our TRF results. Umbelliferone excited state dynamics on the other hand shows that the phototautomer dominates the emission in the region of the pK_a^* [10]. Scopoletin presents another contrast among natural coumarins, where the phototautomer is not observed to play a significant role in the fluorescent emission.

The relative quantum yield of ABC fluorescence compared to aesculetin at pH 8.5 is 1.4 ± 0.2. The most dramatic influence of boric acid on aesculetin fluorescence can be demonstrated at pH ~ 6, which is ~ 1 pH unit below pK_{a1} and where aesculetin by itself has a diminished emission. Figure 6 shows the shift in absorbance and emission with increasing amounts of boric acid buffered at pH 6.1. The addition of boric acid under these conditions increases the total fluorescent emission by a factor of 5, largely because the poorly fluorescent aesculetin neutral becomes the reasonably fluorescent complex. It only takes 2 mM boric acid to double the fluorescence of aesculetin at this pH. At higher pH, the effect is not expected to be nearly as dramatic because the quantum yield of aesculetin improves, becoming like ABC. The behavior documented in Fig. 6 is like the interaction of aesculetin with a diphenylborinic acid compound (the so-called Naturstoff reagent) that enhances the fluorescent emission of aesculetin by more than a factor of ten [26] explained by the formation of a complex like that shown in Scheme 2.

Time-Resolved Fluorescence and Excited-State pK_a

The time-resolved fluorescence of neutral aesculetin allows for direct observation of how excited-state proton transfer influences its emission in the cases where ESPT is competitive with or much faster than fluorescent emission. Placing aesculetin in D_2O effectively deuterates the acidic proton and is expected to slow the ESPT process due to the deuteron's increased mass. Figure 7 shows the time-resolved fluorescence decay of both aesculetin and umbelliferone in water and D_2O – umbelliferone is included as a reference since its fluorescence and kinetic isotope effect has been already described in the literature [7]. The solutions are buffered well below the pK_a of both compounds (pH 4.3 and 4.8 and for H_2O and D_2O, respectively) such that absorbance is by the neutral form, and the emission wavelength is selected to observe primarily neutral emission. Aesculetin N emission (410 nm), represented by trace a (H_2O) and trace b (D_2O), reveals that isotopic substitution slows the decay. Similarly, umbelliferone emission (380 nm), trace c (H_2O) and trace d (D_2O), shows a kinetic isotope effect. The aesculetin

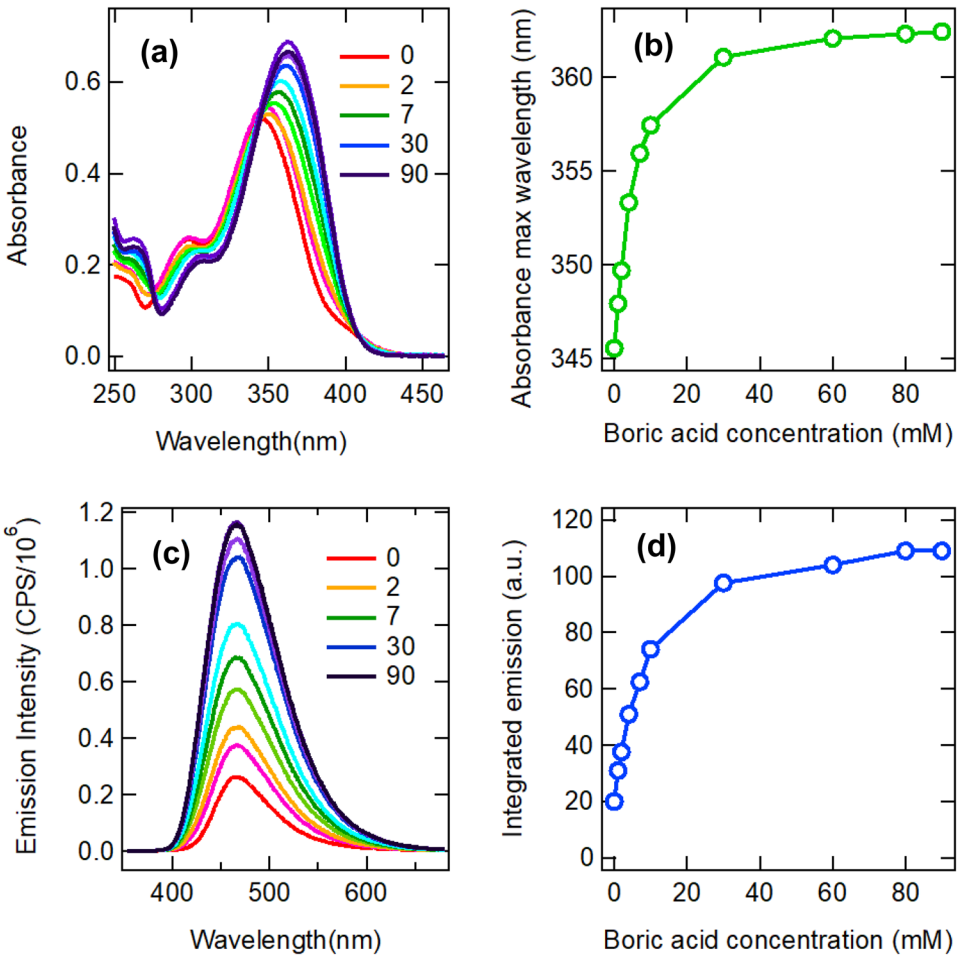

Fig. 6 The effect of boric acid addition to aesculetin buffered at pH 6.1; aesculetin concentration is ~ 50 µM; **panel-a** shows the change in absorbance with boric acid concentration indicated in mM units; **panel-b** shows the change in absorbance maximum wavelength with boric acid concentration; **panel-c** shows fluorescence emission spectra with boric acid concentration indicated in mM units, the excitation wavelength is 347 nm corresponding to the iso-absorbance point; **panel-d** shows the change in total fluorescence intensity as the integrated curves from **panel-c** with boric acid concentration

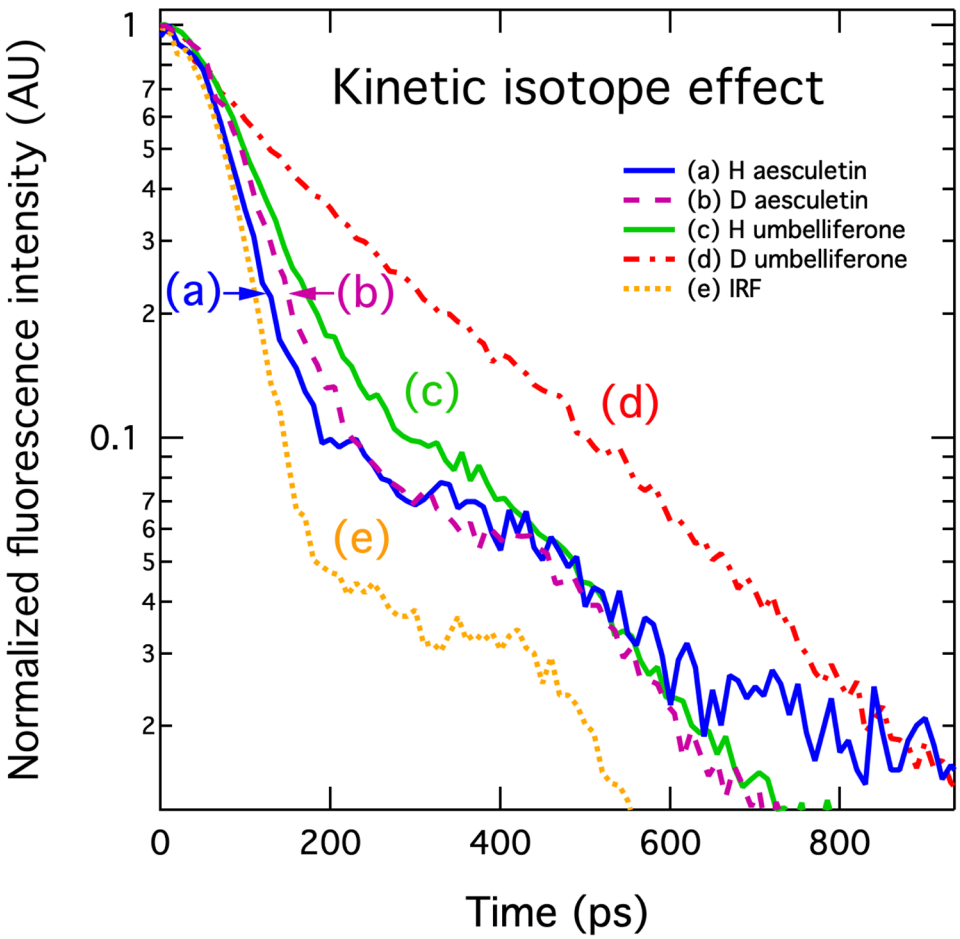

Fig. 7 Time-resolved fluorescence decay curves showing the kinetic isotope effect for aesculetin and umbelliferone; all solutions are 0.1 M citrate buffer prepared in either H_2O (pH 4.3) or D_2O (pH 4.8); (**a**) solid, blue trace, aesculetin in H_2O, (**b**) dashed, violet trace, aesculetin in D_2O, (**c**) solid, green trace, umbelliferone in H_2O, (**d**) dot-dash, red trace, umbelliferone in D_2O, and (**e**) dotted, orange trace, instrument response function

decays are faster than those due to umbelliferone. These fast decays are fitted by exponential curves in convolution with the instrument response function (IRF, Fig. 7 trace e) to give aesculetin N fluorescence lifetimes (τ_H and τ_D) of 19 and 55 ps, respectively (listed in Table 3, Fig. S7 shows the fit results with residuals). The umbelliferone τ_H and τ_D, based on the Fig. 7 decays, are 65 and 200 ps, respectively, which compare well to previously reported corresponding lifetimes [7] of 48 ps and 155 ps. Clearly the ESPT process is faster in aesculetin compared to umbelliferone. The most straightforward model for these short lifetimes is that the ESPT process is much faster than the fluorescence lifetime and the observed decay constant is essentially the ESPT rate constant.

The kinetic isotope effect (KIE, τ_D/τ_H) slows the aesculetin ESPT rate by a factor of about 3, which agrees well with the KIE reported for umbelliferone [19]. The inverses of these lifetime values give aesculetin rate constants (k_{PT}) of 5.3×10^{10} s^{-1} and 1.8×10^{10} s^{-1}, for H_2O and D_2O respectively. The lifetime of neutral aesculetin is considerably shorter than that of neutral scopoletin (0.5 ns, $k_{PT}=2\times10^{9}$ s^{-1}) [8]. Pines et al. propose a kinetic isotope effect of 3 for strong photoacids such as umbelliferone and aesculetin [27], agreeing well with our KIE for aesculetin. Pinto da Silva et al. describe a linear relationship between log(k_{PT}) and pK_a^* for photoacids, including two hydroxycoumarins, having pK_a^* values in the range 0 to 3 [28]. Our observed N-emission lifetime matches the low pK_a^* end of that linear relationship putting the value of aesculetin pK_{a1}^* at 0. It is clearly faster than umbelliferone, which has $k_{PT}=2\times10^{10}$ s^{-1} and pK_a^* of 0.4 [19], and

Table 3 Fluorescence lifetimes of aesculetin, molecular forms are neutral, N; anion, A; and tautomer, T

pH/Solvent	Molecular form	Excitation λ (nm)	Emission λ (nm)	Lifetime (ps)
4.3, H_2O	N	345	410	19 ± 2
4.8, D_2O	N	345	410	55 ± 0.5
5, H_2O	A	350	470	2.30×10^3
5, H_2O	T	350	600	150 ± 25
9, H_2O	A	350	460	2.16×10^3
			470	2.26×10^3
Methanol	N	350	460	2.76×10^3
Ethanol	N	350	460	3.75×10^3

hence it is reasonable that aesculetin has a lower pK_a^* than umbelliferone. Pines [27] shows how $\log(k_{PT})$ versus pK_a^* becomes nonlinear for pK_a^* below 0 for a collection of phenol-type photoacids and, projecting our $\log(k_{PT}) = 10.7$ on this curve, predicts a pK_{a1}^* for aesculetin near –2. Taking both relationships into account, our time resolved data indicates an aesculetin pK_{a1}^* of -1 ± 1, making it one of the strongest natural coumarin photoacids studied.

Compounds can be considered strong photoacids when their pK_a^* values are seven or more pH units lower than the ground state pK_a, meaning their acid ionization constant becomes at least seven orders of magnitude larger after photoexcitation [29]. The $\Delta pK_a = pK_a - pK_a^*$ of aesculetin is 8.3, which is larger than the ~ 7.4 for umbelliferone, although these are perhaps not significantly different based on uncertainty. Another gauge of photoacid strength is whether in fact the light absorption transforms a weak acid into a strong acid, in this case having a $pK_a^* \leq 0$.

Table 3 also contains lifetimes for the aesculetin anion emission (~ 560 nm) below and above the pK_a, emission at 600 nm at pH 5 (attributed to the phototautomer), and aesculetin fluorescence in methanol and ethanol (Figs. S8 and S9 show fits and residuals). The aesculetin anion lifetime is about half of the ~ 5 ns lifetime of scopoletin anion [8, 12] and umbelliferone anion [7] in aqueous media, which is qualitatively consistent with the lower quantum yield of aesculetin anion. The lifetime of the phototautomer is intermediate between the neutral and anion, almost ten-fold slower than the proton transfer process based on a weak signal. Further study of this emission should include observing a kinetic isotope effect. The aesculetin-borate ion complex fluorescence lifetime is 1.6 ± 0.1 ns (Fig. S10).

Modeling Results

Modeling the absorbance and emission spectra of all the aesculetin species in aqueous solution discussed in this paper using DFT/TD-DFT methods shows good agreement with experimental spectra. Figure S11 shows experimental and modeled aqueous spectra. A modest level of DFT modeling predicts the correct location of the ABC absorbance maximum between the aesculetin neutral and anion absorbance and the overlap of the ABC and anion emission spectra. The modeling also reproduces the observation that the dianion has a large red shift from the anion compared to the neutral-anion red shift in both absorbance and emission spectra. It also predicts the tautomer emission is red shifted relative to the anion, although the agreement is only qualitative in this case.

Table S2 shows the frontier molecular orbitals (highest occupied molecular orbital, HOMO, and lowest unoccupied molecular orbital, LUMO) for the five aesculetin species in the gas phase. These reveal a common motif of HOMO electron density centered on the benzene ring shifting in the excited-state LUMO to the pyrone ring, representing an intramolecular charge transfer. It is expected that solvent polarity will affect the position of the spectral band maxima. If the excited state dipole is larger than the ground state, a more polar solvent will have a stabilizing effect, reducing the difference in energy between the states, and will manifest as a red shift of the absorbance band comparing spectra from less to more polar solvents. For example, aesculetin absorbance in ethanol is redshifted with respect to umbelliferone due to this effect [30]. Further study of the aesculetin borate complex in solvents of different polarity may provide additional insight to its photophysical behavior.

Conclusion

The data presented here give a clear picture of the photophysical properties of aesculetin and the complex it forms with boric acid. Aesculetin is a stronger photoacid than umbelliferone. It has a pK_{a1}^* lower than umbelliferone and a similar but somewhat larger ΔpK_a than umbelliferone. The strong pH dependence of the relative quantum yield, appearing closely related to pK_a, sets aesculetin apart from the similar fluorescent, natural coumarins, umbelliferone and scopoletin, suggesting there may be unique structural functionality of the vicinal hydroxyl groups of aesculetin. The anion of aesculetin exhibits weak photobase character. When aesculetin is aqueous solution with boric acid, a fluorescent complex is formed with pK_c of 5.6.

Supplementary Information The online version contains supplementary material available at https://doi.org/10.1007/s10895-021-02842-w.

Acknowledgements The authors are grateful for the following support: We thank Dr. Gary Blanchard, Michigan State University, for his generous time, collaboration and providing access to his TRF system and MSU colleague, Jessica Kline, for data analysis. The MSU Mass Spectrometry and Metabolomics Core provided LC-high resolution mass spec data.

Authors' Contributions LHK edited the draft for general write up and performed the experiments, GRD performed DFT modeling, IBJ, LPH, YT, and JY performed the experiments, MAM wrote the manuscript in consultation with the other co-authors.

Funding National Science Foundation grant 1956223, Beckman Scholars Program (LK), NSF-funded Calvin Computer cluster (MRI-grant 1726260), Calvin Research Fellowship program (MM), the Storteboom Summer Research Fellowship (YT, 2018), the Enno Wolthuis Summer Research Fellowship (YT, 2019), Luke and Pauline Schaap Summer Research Fellowship (GD), the Thedford P. Dirkse Summer Science Research Fellowship (HP, 2018; IJ, 2021)

Data Availability All data generated or analyzed during this study are included in this published article and its supplementary information

Declarations

Ethics Approval not applicable

Consent to Participate not applicable

Consent for Publication not applicable

Conflicts of Interest/Competing Interests the authors declare no conflicts of interest or competing interests.

References

1. Pruccoli L, Morroni F, Sita G et al (2020) Esculetin as a Bifunctional Antioxidant Prevents and Counteracts the Oxidative Stress and Neuronal Death Induced by Amyloid Protein in SH-SY5Y Cells. Antioxid 9:551. https://doi.org/10.3390/antiox9060551
2. Dong Y, Hou Q, Sun M et al (2020) Targeted Isolation of Antioxidant Constituents from Plantago asiatica L. and In Vitro Activity Assay. Molecules 25:1825. https://doi.org/10.3390/molecules25081825
3. Cao D, Liu Z, Verwilst P et al (2019) Coumarin-Based Small-Molecule Fluorescent Chemosensors. Chem Rev 119:10403–10519. https://doi.org/10.1021/acs.chemrev.9b00145
4. Zhang H-Y, Wang L-F (2004) Theoretical elucidation of structure–activity relationship for coumarins to scavenge peroxyl radical. J Mol Struct THEOCHEM 673:199–202. https://doi.org/10.1016/j.theochem.2003.12.014
5. Signore G, Nifosì R, Albertazzi L et al (2010) Polarity-Sensitive Coumarins Tailored to Live Cell Imaging. J Am Chem Soc 132:1276–1288. https://doi.org/10.1021/ja9050444
6. Nowak PM, Woźniakiewicz M, Piwowarska M, Kościelniak P (2016) Determination of acid dissociation constant of 20 coumarin derivatives by capillary electrophoresis using the amine capillary and two different methodologies. J Chromatogr A 1446:149–157. https://doi.org/10.1016/j.chroma.2016.03.084
7. Simkovitch R, Huppert D (2015) Photoprotolytic Processes of Umbelliferone and Proposed Function in Resistance to Fungal Infection. J Phys Chem B 119:14683–14696. https://doi.org/10.1021/acs.jpcb.5b08439
8. Pham HT, Yoo J, VandenBerg M, Muyskens MA (2020) Fluorescence of Scopoletin Including its Photoacidity and Large Stokes Shift. J Fluoresc 30:71–80. https://doi.org/10.1007/s10895-019-02471-4
9. Reijenga J, van Hoof A, van Loon A, Teunissen B (2013) Development of Methods for the Determination of pKa Values. Anal Chem Insights 8:53–71. https://doi.org/10.4137/ACI.S12304
10. Moriya T (1983) Excited-state Reactions of Coumarins in Aqueous Solutions. I. The Phototautomerization of 7-Hydroxycoumarin and Its Derivative. Bull Chem Soc Jpn 56:6–14. https://doi.org/10.1246/bcsj.56.6
11. Schulman SG, Rosenberg LS (1979) Tautomerization kinetics of 7-hydroxy-4-methylcoumarin in the lowest excited singlet state. J Phys Chem 83:447–451. https://doi.org/10.1021/j100467a005
12. Pina J, de Castro CS, Delgado-Pinar E, Seixas S, de Melo J (2019) Characterization of 4-methylesculetin and of its mono- and di-methoxylated derivatives in water and organic solvents in its ground, singlet and triplet excited states. J Mol Liq 278:616–626. https://doi.org/10.1016/j.molliq.2019.01.083
13. Grzywacz J, Taszner S (1982) Influence of pH on the Absorption and Fluorescence Spectra of 6,7-Dihydroxycoumarin in Aqueous Solution. Z Für Naturforschung A 37:262–265. https://doi.org/10.1515/zna-1982-0311
14. Mongay C, Cerda V (1974) A Britton-Robinson Buffer of Known Ionic Strength. Ann Chim 64:409–412
15. Lakowicz JR (2006) Principles of Fluorescence Spectroscopy, 3rd edn. Springer, US
16. Frisch M, Trucks G, Schlegel H et al (2016) Gaussian 16, Revision B.01. Gaussian, Inc., Wallingford, CT
17. Schmidt J, Polik W WebMO Pro. WebMO, LLC, Holland, MI, USA. Available from http://www.webmo.net
18. Richard P, Lucia B (1977) Mechanism of the complexation of boron acids with catechol and substituted catechols. Inorg Chem 16:1677–1681. https://doi.org/10.1021/ic50173a021
19. Simkovitch R, Pinto da Silva L, Esteves da Silva JCG, Huppert D (2016) Comparison of the Photoprotolytic Processes of Three 7-Hydroxycoumarins. J Phys Chem B 120:10297–10310. https://doi.org/10.1021/acs.jpcb.6b01383
20. Houari Y, Jacquemin D, Laurent AD (2013) TD-DFT study of the pKa∗ for coumarins. Chem Phys Lett 583:218–221. https://doi.org/10.1016/j.cplett.2013.08.002
21. Ferrari AM, Sgobba M, Gamberini MC, Rastelli G (2007) Relationship between quantum-chemical descriptors of proton dissociation and experimental acidity constants of various hydroxylated coumarins. Identification of the biologically active species for xanthine oxidase inhibition. Eur J Med Chem 42:1028–1031. https://doi.org/10.1016/j.ejmech.2006.12.023
22. Goodwin RH, Kavanagh F (1950) Fluorescence of coumarin derivatives as a function of pH. Arch Biochem 27:152–173
23. Zhang J, Liu C, Wei Y (2011) Fluorescence quantum yield and ionization constant of umbelliferone. Chem Bull Huaxue Tongbao 74:957–960
24. Pines E, Fleming GR (1994) Self quenching of 1-naphthol. Connection between time-resolved and steady-state measurements. Chem Phys 183:393–402. https://doi.org/10.1016/0301-0104(94)00098-0
25. Jones G, Jackson WR, Choi CY, Bergmark WR (1985) Solvent effects on emission yield and lifetime for coumarin laser dyes. Requirements for a rotatory decay mechanism. J Phys Chem 89:294–300. https://doi.org/10.1021/j100248a024
26. Tattini M, Di Ferdinando M, Brunetti C et al (2014) Esculetin and esculin (esculetin 6-O-glucoside) occur as inclusions and are differentially distributed in the vacuole of palisade cells in Fraxinus ornus leaves: A fluorescence microscopy analysis. J Photochem Photobiol B 140:28–35. https://doi.org/10.1016/j.jphotobiol.2014.06.012
27. Pines E (2005) The Kinetic Isotope Effect in the Photo-Dissociation Reaction of Excited-State Acids in Aqueous Solutions. Isotope Effects in Chemistry and Biology. CRC Press LLC, Boca Raton, Fla, pp 451–464
28. Pinto da Silva L, Simkovitch R, Huppert D, Esteves da Silva JCG (2017) Combined experimental and theoretical study of the photochemistry of 4- and 3-hydroxycoumarin. J Photochem Photobiol Chem 338:23–36. https://doi.org/10.1016/j.jphotochem.2017.01.032
29. Cohen B, Huppert D (2001) Excited State Proton-Transfer Reactions of Coumarin 4 in Protic Solvents. J Phys Chem A 105:7157–7164. https://doi.org/10.1021/jp010576q
30. Abu-Eittah RH, El-Tawil BAH (1985) The electronic absorption spectra of some coumarins. A molecular orbital treatment. Can J Chem 63:1173–1179. https://doi.org/10.1139/v85-200